Journal of Analytical and Applied Pyrolysis 179 (2024) 106463

Contents lists available at ScienceDirect

Journal of Analytical and Applied Pyrolysis

journal homepage: www.elsevier.com/locate/jaap

Impact of high-temperature biomass pyrolysis on biochar formation and composition

Xun Zou [a,b], Paulo Debiagi [c,d], Muhammad Ahsan Amjed [e], Ming Zhai [a,b,*], Tiziano Faravelli [e,**]

[a] School of Energy Science and Engineering, Harbin Institute of Technology, Harbin, Heilongjiang 150001, China
[b] Heilongjiang Key Laboratory of New Energy Storage Materials and Process, Harbin, Heilongjiang, 150001, China
[c] Technical University of Darmstadt, Department of Mechanical Engineering, Simulation of reactive Thermo-Fluid Systems, Otto-Berndt-Str. 2, Darmstadt 64287, Germany
[d] Nottingham Ningbo China Beacons of Excellence Research and Innovation Institute, University of Nottingham Ningbo China, Ningbo, China
[e] Politecnico di Milano, Department of Chemistry, Materials and Chemical Engineering "G. Natta", CRECK Modelling Lab, Milano 20133, Italy

ARTICLE INFO

Keywords:
TGA-MS
Biochar
High-temperature pyrolysis
Kinetic mechanism
Oxygen functionalities
CRECK-S-B

ABSTRACT

The development and utilization of biomass play a vital role in reducing fossil fuel dependency and mitigating greenhouse gas emissions. High-temperature pyrolysis provides a promising route for converting biomass into valuable products without tar formation. Kinetic models are essential for understanding biomass pyrolysis processes, aiding reactor design and optimization. In this study, rice husk (RH) and corn straw (CS) are selected, which exhibit significant differences in ash content but are widely present. Pyrolysis is performed using a thermogravimetric analyzer coupled with a mass spectrometer (TGA-MS). The results show a rapid decrease in solid residue oxygen content at elevated temperatures, which stabilized after reaching 900°C, accounting for about 8–10%. MS quantification indicates increased release of H_2O and CO during this stage. Fourier transform infrared spectroscopy (FTIR) analysis on the biochar unveils that this phenomenon is attributed to the stretching vibration of C-O bonds and the conversion of -OH groups. The remaining oxygen primarily exists as carbonyl and carboxyl groups. Subsequently, the CRECK-S-B biomass pyrolysis kinetic model is updated, specifically targeting the transformation mechanism of oxygen-containing solids at high temperatures to improve the prediction of biochar yield and elemental composition. The relative error of oxygen content prediction is less than 10%. The accuracy of the model is validated through experimental data and an extensive literature database, leading to the establishment of a comprehensive database. The updated model demonstrates significantly enhanced prediction accuracy for pyrolysis temperatures above 800°C, expanding its applicability range. Moreover, it achieves an accuracy rate exceeding 80% for char yield and elemental content in the temperature range of 200–1000°C, including torrefaction conditions. It provides a theoretical foundation for the effective utilization of high-temperature biochar, offers a novel insight into biomass thermochemical conversion, and contributes to the sustainable development of biomass energy.

1. Introduction

The development and utilization of novel energy sources have become imperative to address the urgent need to reduce human reliance on fossil fuels [1]. Biomass, as a type of renewable energy, has garnered significant attention due to its abundant reserves and wide availability [2–5]. The generation and processing of biomass offer a net-zero emissions process, positioning it as one of the most promising energy alternatives of the 21st century [6,7]. Among the utilization pathways of biomass, pyrolysis is recognized as a potential substitute for co-production technologies [8,9]. It enables the production of various chemicals, biochar, pyrolysis gases, and bio-oil, showcasing strong sustainability and low greenhouse gas emissions [10–12]. The solid product obtained from biomass pyrolysis, known as biochar, exhibits high surface activity [13,14]. Biochar can be directly utilized as fuel or employed as a feedstock for gasification-based power generation. Additionally, biochar serves as a versatile material, finding applications in soil amendment, as a fuel cell electrode, and as an excellent choice for energy storage [15–17].

* Corresponding author at: School of Energy Science and Engineering, Harbin Institute of Technology, Harbin, Heilongjiang 150001, China.
** Corresponding author.
E-mail addresses: zhaiming@hit.edu.cn (M. Zhai), tiziano.faravelli@polimi.it (T. Faravelli).

https://doi.org/10.1016/j.jaap.2024.106463
Received 15 January 2024; Received in revised form 4 March 2024; Accepted 13 March 2024
Available online 16 March 2024

Nomenclature

Abbreviations

ad	air-dry basis
A	Ash
daf	dry, ash-free basis
FC	Fixed carbon
LIG	Lignin
M	Moisture
RH	Rice Husk
V	Volatile
AAEMs	Alkali and alkaline earth metal elements
CS	Corn Straw
dTG	Derivative thermogravimetric
FTIR	Fourier transform infrared spectroscopy
m/z	Mass-to-charge ratios
MS	Mass spectrometer
SM	Supplemental material
TGA	Thermogravimetric analyzer

The high-temperature pyrolysis of biomass provides the necessary activation energy to break covalent bonds, resulting in the production of low molecular weight substances and high-calorific value gas products. According to reports [18], biomass can be converted into gas at rates as high as 87 wt% when the temperature exceeds 800–1000°C. Caglar et al. [19] observed an increase in combustible gas content with rising pyrolysis temperature. Efika et al. [20] considered that high-temperature pyrolysis enhances the cracking of larger volatiles (tars), leading to higher yields of high-calorific value gas products. Additionally, high-temperature pyrolysis can also prove to be an effective approach in mitigating the challenges related to tar formation. In our previous study [21], the tar yield reached the milligram level and became negligible when the pyrolysis temperature exceeded 900℃. Septien et al. [22] conducted experiments in an entrained-flow bed reactor and demonstrated biomass conversion into tar-free high-value products through high-temperature fast pyrolysis. The results of Paethanom et al. [23] show that the tar removal ability is significantly influenced by the pyrolysis temperature, with tar removal rates reaching 87.5% at 800°C. Biochar at high temperatures tends to exhibit orderliness and uniformity, making it more targeted for specific applications [24,25]. Pariyar et al. [26] proposed that biochar prepared at higher temperatures is more suitable for carbon sequestration. Anand et al. [27] suggest that biochar above 800°C possesses high micropore volume and aromaticity. Its surface oxygen functional groups and large surface area make it an effective adsorbent for removing pollutants, particularly in aquatic systems contaminated with heavy metals and organic pollutants. Surup et al. [28] found that high-temperature wood char can be successfully used as a substitute for fossil-based reducing agents in the metallurgical industry, reducing costs and environmental pollution. Therefore, acquiring a comprehensive understanding of the high-temperature pyrolysis process of biomass is crucial.

The products of high-temperature pyrolysis have different applications and offer targeted benefits. Therefore, studying pyrolysis kinetics not only reveals the reaction mechanisms but also paves the way for novel pyrolysis-based approaches for efficient biomass utilization, presenting significant scientific research value and engineering prospects.

Assessing biomass pyrolysis kinetics is crucial for understanding the process and determining its controlling parameters. It directly relates to the thermochemical utilization of biomass, providing insights into the reaction pathways or mechanisms and enabling the prediction of reaction rates and complexity [29,30]. Regrettably, current research is deficient in a comprehensive kinetic model that elucidates the intricacies of the high-temperature pyrolysis process of biomass. With the advent of high-performance computers, advanced kinetic methods and molecular simulations have been widely employed, leading to comprehensive mechanistic models such as the semi-detailed lumped kinetic model [31]. The lumped kinetic model describes solid conversion, gas release, and devolatilization reactions based on three reference components of biomass [32,33]. The accuracy of the models is validated by comparing predicted biomass mass loss rates and pyrolysis product distribution with experimental data. The established multi-step reaction models have many applications for different biomass feedstocks and pyrolysis conditions [34], making them the optimal choice for investigating high-temperature biomass pyrolysis kinetics.

Motivated by these facts, two biomass feedstocks containing different amounts of ashes were selected to investigate their pyrolysis behavior and characterize biochar formation at high temperatures. Experiments are conducted in two different pyrolysis systems: a high-temperature, fixed-bed reactor for isothermal experiments and a thermogravimetric analyzer coupled with mass spectrometry (TGA-MS) for non-isothermal experiments. Ultimate and FTIR analyses are conducted on the high-temperature biochars. The CRECK-S-B model is employed to numerically reproduce the pyrolysis processes. Through comparison of the experimental data together with relevant literature and sensitivity analysis, improvements are proposed to the model to account for the high-temperature evidences observed in the experiments. The updated model is then validated with a large collection of literature experimental data, which is organized and made available as a database in the supplemental material. This work aims at presenting new data of high-temperature pyrolysis of biomass and to establish a kinetic model of this process, offering a novel insight into the thermochemical utilization of biomass and contributing to the sustainable development of biomass energy.

The work is organized as follows: In Section 2 the materials experimental methods are described. In Section 3 the experimental findings are reported and discussed. In Section 4, the modeling activity is described, comparing the experimental results with the kinetic model predictions, followed by the improvements and validation of the model. Final comments and conclusions are drawn in Section 5.

2. Methodology

2.1. Materials

Rice husk (RH) and corn straw (CS) samples from Heilongjiang Province, China, were selected for the experimental study. They are two representative biomass feedstocks of widely different ash contents. Table 1 summarizes the proximate and ultimate analyses. The C, H, O, and N contents of the raw materials are measured by the micro-combustion method in the elemental analyzer (Vario EK III) [35]. The biomass biochemical composition is determined by the characterization method from Debiagi et al. [32] to characterize the samples using the ultimate analysis.

2.2. Apparatus and Procedures

2.2.1. Sample preparation

The biomass raw materials were finely grounded, followed by sieving through a 20-mesh to retain particles smaller than 0.85 mm. Samples were dried in an oven at 105℃ for 12 hours.

2.2.2. High-temperature pyrolysis system

The pyrolysis process was carried out in a self-designed high-temperature pyrolysis experimental system, (Fig. 1). The main body of the pyrolysis reaction chamber is a cylindrical alumina tube with a length of 1000 mm and an inner diameter of 60 mm. The heating unit consists of eight "U"-shaped silicon molybdenum rods, type B thermocouples, and a programmable logic controller. The temperature could be controlled within the range of 25–1600°C. The experimental gas was supplied from

Table 1
The proximate, ultimate analysis and biochemical composition of biomass.

Biomass	Proximate analysis (*wt%*)				Ultimate analysis (*wt%*)				Biochemical composition (*wt%*)		
	M_{ad}	V_{ad}	A_{ad}	FC_{ad}	C_{daf}	H_{daf}	O_{daf}	N_{daf}	$CELL_{daf}$	$HCELL_{daf}$	LIG_{daf}
RH	2.8	62.7	18.8	15.7	46.5	6.1	46.7	0.7	46.2	42.4	7.1
CS	4.4	75.9	2.6	17.1	45.8	6.0	47.3	0.9	46.2	44.9	5.6

Note: M= moisture, V= volatile, A= ash, FC= fixed carbon, ad= air-dry basis, daf=, CELL= cellulose, HCELL= hemicellulose, LIG= lignin.

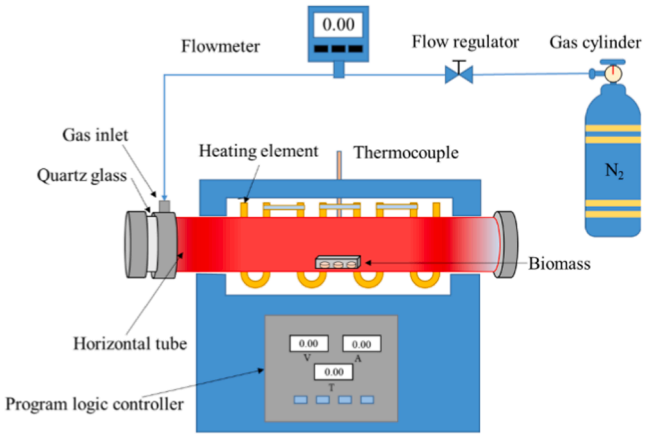

Fig. 1. High-temperature pyrolysis system.

high-pressure cylinders. To ensure a stable and oxygen-free environment, the furnace was preheated in an N_2 atmosphere to the desired pyrolysis temperature and held for 2 hours. A sample weighing 2 g was placed in a crucible, while the N_2 flow rate was set at 20 L/min. Subsequently, the crucible was promptly positioned at the center of the constant temperature zone for a 10-minute pyrolysis period. Upon completion of the pyrolysis process, the crucible was moved to the quartz glass at the end of the corundum tube and cooled under an N_2 atmosphere. Biochar samples were collected for further analysis.

2.2.3. TGA-MS Analysis

Pyrolysis of the raw biomasses was also conducted in a thermogravimetric analyzer (TGA STA449C, Netzsch, Germany) coupled with a mass spectrometer (MS QMS403, Netzsch, Germany). For each experiment, approximately 5–10 mg of the sample was used, and TGA was conducted under a controlled argon gas atmosphere, flowing at a rate of 100 ml/min. The heating rate was 20 ℃/min, while the target temperature reached 1000℃. The volatiles released in the TGA were transferred through a heated line that was interfaced with the MS. Operating under vacuum conditions, the MS detected and measured the characteristic fragment ion intensities of the volatiles based on their respective mass-to-charge ratios (m/z).

2.2.4. FTIR Analysis

The infrared spectrum of the biochars was analyzed using a Nicolet 5700 FTIR spectrometer. The biochar samples were dried at 105℃ in an oven for 12 hours, followed by thorough mixing, grinding, and pelletizing with a mass ratio of 1:120 using spectroscopic grade KBr. The recorded infrared spectra spanned a range of 400 cm^{-1} to 4000 cm^{-1} with a resolution of 4 cm^{-1}. Each spectrum was scanned 32 times to generate the infrared spectrum curve of the biochar. The composition and content of functional groups in the sample were determined by analyzing the characteristic absorption peaks in the spectra, considering their positions and relative intensities.

3. Experimental results and discussion

3.1. TG-MS Analysis

Fig. 2 illustrates the thermogravimetric (TG) and derivative thermogravimetric (dTG) curves. The initial stage corresponds to the dehydration and drying of the biomass, occurring between 75 and 150℃. The onset of decomposition for both types of biomass takes place within the temperature range of 300–400℃. This process is attributed to the release of volatile components primarily derived from the decomposition of hemicellulose and cellulose [36]. Lignin decomposition takes place at a wider temperature range, first overlapping with the other components and later characterizing the mass loss at 400–500℃. At temperatures within 500–700℃, the mass loss is attributed to the biochar decomposition, releasing light gases. Aromatic compounds grow forming Polycyclic Aromatic Hydrocarbons, resulting in the formation of multi-ring structures. As the pyrolysis temperature continues to rise, mass loss tends to stabilize at 900℃. Within the temperature ranges of 700–1000℃, the respective mass losses are 1.1% and 1.5%. Overall, CS exhibits a higher mass loss than RH, possibly due to the higher ash content in RH. The dTG results reveal that the pyrolysis process cannot be described as a single component thermal conversion. The differences in peak heights and positions indicate a strong correlation between the thermal stability of biomass and its chemical structure. The peak of mass loss for RH and CS occur at 354.3℃ and 334.1℃, respectively, corresponding to the cellulose decomposition. Furthermore, an additional peak is observed for CS at 206.4℃, displaying a weight loss rate of 5.87%/min. This peak can be attributed to the release of light volatile components, possibly arising from the higher hemicellulose content in CS. The shoulder in RH devolatilization corresponds to hemicellulose, and the different temperature for this peak when compared to CS indicates the different nature of the hemicelluloses. The above findings comprehensively demonstrate the influence of different organic and inorganic constituents of biomass on the pyrolysis process.

With the assistance of MS spectra, the chemical composition of the evolved gases during different decomposition steps was elucidated by comparing the peak intensities corresponding to different m/z (Fig. 3). The intensities of several major gas species released during the pyrolysis processes, including H_2, CH_4, H_2O, CO, CH_2O, and CO_2, were detected and analyzed. The ion intensity and release process of H_2 in the pyrolysis gases of both biomass types exhibit a remarkable similarity. Especially two distinct peaks were observed at low temperatures (300–400℃) and high temperatures (700–800℃). The former peak was attributed to the decomposition of C-H groups in cellulose. The other peak was potentially associated with the reforming reaction of CH_4 during the pyrolysis process, leading to a reduction in CH_4 intensity within that temperature range. The release peak of CH_4 coincided with the decomposition stages of three main components, primarily arising from the removal of methoxy substituents and the cleavage of aliphatic carbon chains. According to the ion intensity results, the release of H_2O can be divided into multiple stages. Initially, at around 100°C, moisture is removed. The subsequent peak corresponds to the desorption of hydroxyl groups. In the decomposition of lignin, the transformation of aromatic alkyl/hydroxyl substitutes and dehydration reactions play a significant role in the production of H_2O. It is noteworthy that at pyrolysis temperatures above 700°C, there is a slight increase in the intensity of H_2O, suggesting further conversion of oxygen-containing functional groups. The

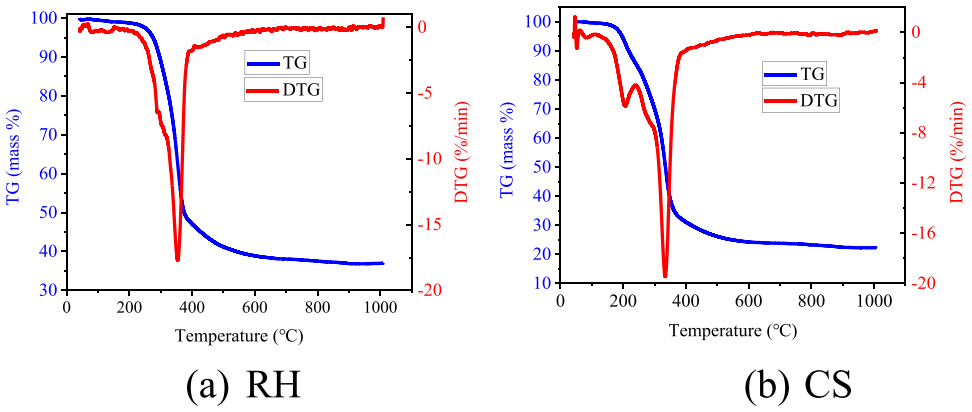

Fig. 2. TG and DTG curves of the biomass.

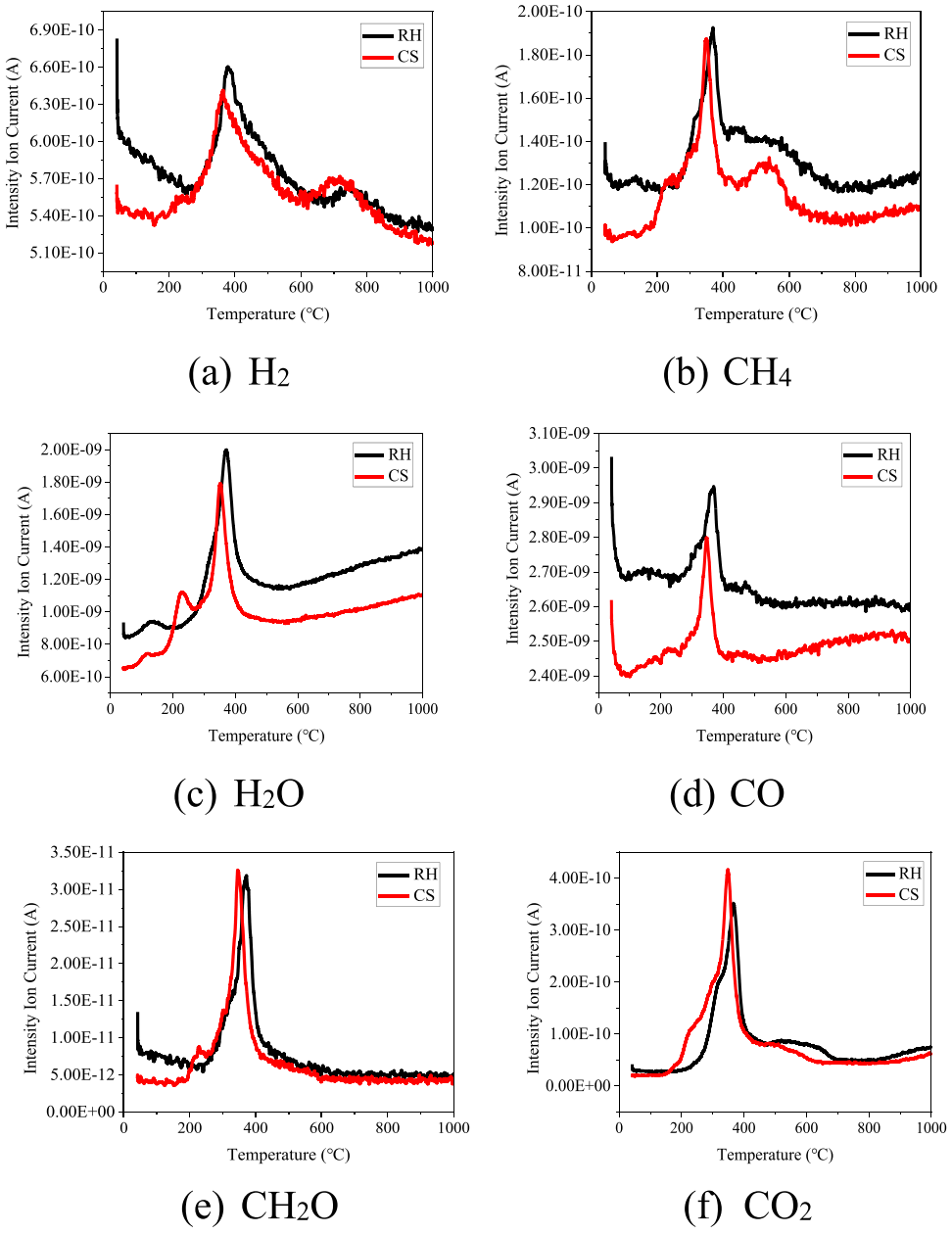

Fig. 3. MS spectrogram of the biomass.

additional peak observed in CS aligns with TGA, providing consistent results. The use of argon gas in the pyrolysis atmosphere eliminates interference from nitrogen gas, with the *m/z*=28 peak identified as CO. Among the gases released, CO exhibits the highest ion intensity. Its peak occurs during the decomposition stages of hemicellulose and cellulose, primarily resulting from the cleavage of C-O-C and C═O groups. The width of the CO peak in RH is slightly broader compared to CS, but it becomes stable at higher temperatures. The ion intensity of CO in CS shows an upward trend above 600°C, potentially due to secondary reactions and cracking of primary pyrolysis-generated biochar. Consequently, within this temperature range, CS demonstrates a slightly higher biochar yield reduction rate than RH. The ion intensities and distributions of CH_2O, the major pyrolysis gases with the lowest yields, are relatively similar between the two biomass types, with only a slightly earlier release of CH_2O in CS compared to RH. The release of CO_2 is believed to be influenced by reaction rates [37]. As indicated by TGA, the elevated thermal loss rate of CS elucidates the preferential release and higher peak intensity of CO_2. The minor peak observed at 600°C can be attributed to some macromolecular cracking. Similarly, the ion intensity slightly increases after 800°C, possibly stemming from the decomposition of carbonyl and carboxyl groups. Except for CO_2, the quantity of gases produced during RH pyrolysis exceeds that of CS, while CS leaves a higher solid residue. It is evident that the total yield of tar and non-condensable gases in CS pyrolysis is anticipated to be higher than that in RH.

3.2. Biochar characteristics

Fig. 4 shows the char yield of both biomass types at various pyrolysis temperatures. The char yield of RH decreases from 41.2% at 500°C to 36.9% as the temperature increases. Similarly, CS exhibits a decrease from 26.2% to 22.3%, with a change slightly lower than that of RH. Above 900°C, the char yield for both biomass types remains constant and the char yield difference between them remains nearly unchanged. Despite variations in ash content contributing to the differences in char yield, RH and CS show a similar trend in elemental content changes under high-temperature conditions. Table 2 reports the ultimate analyses of the biochars. The biochars obtained from rice husk or corn straw under different pyrolysis temperatures are denoted as "RH-Temperature" or "CS-Temperature." For example, RH-500 represents the biochar produced from rice husk at 500°C.

As anticipated, increasing the pyrolysis temperature leads to a decrease in char yield, accompanied by reductions in the H/C and O/C ratios. The increase in carbon content can primarily be attributed to the formation of polycyclic aromatic hydrocarbon structures resulting from the cyclization of side alkyl chains and from the aggregation of aromatic units in biochar. The decrease in hydrogen and oxygen content is caused mainly by removing hydrogen- and oxygen-containing functional groups, the de-alkylation and the ring-opening reactions of the three biomass components. The rapid decline in oxygen content occurs in two stages, corresponding to the peaks observed in the MS results for releasing CO and CO_2. The O/C ratio of RH decreases at a higher rate than CS because of the slightly higher lignin content in RH. The β-O-4 bond, the main interunit linkage in lignin, tends to decompose under medium pyrolysis temperatures (500–600°C). The O/C ratio remains constant above 900°C, but the H/C ratio continues to decrease, indicating ongoing carbonization of biochar. Moreover, the H/C ratio is slightly higher for RH at each temperature, aligning with Crombie Kyle et al. [38] findings that CS char exhibits greater stability than RH char.

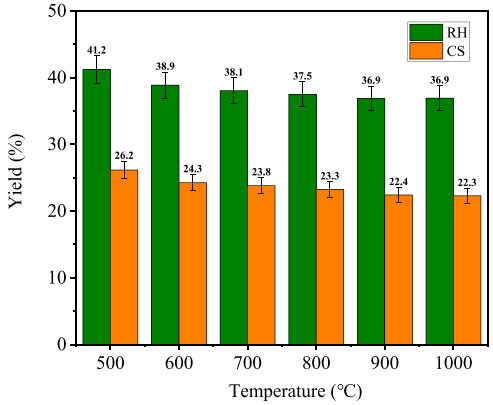

Fig. 4. Yields of biochar.

Table 2
Ultimate analysis of the biochar.

Biochar	Ultimate analysis (daf *wt%*)					Ash (dry *wt%*)	Molar ratio (daf)	
	C_{daf}	H_{daf}	O_{daf}	N_{daf}	S_{daf}	A_{ad}	H/C	O/C
RH-raw	46.5 ± 0.5	6.10 ± 0.05	46.7 ± 0.5	0.69 ± 0.01	0.01 ± 0.01	18.8	1.57	0.75
RH-500	68.1 ± 0.4	3.58 ± 0.01	27.3 ± 0.3	0.98 ± 0.02	0.04 ± 0.01	32.4	0.63	0.30
RH-600	74.1 ± 0.2	2.63 ± 0.02	22.2 ± 0.1	1.01 ± 0.01	0.06 ± 0.01	39.2	0.43	0.22
RH-700	76.6 ± 0.5	2.08 ± 0.01	20.2 ± 0.2	1.07 ± 0.01	0.05 ± 0.01	42.8	0.33	0.20
RH-800	77.6 ± 0.5	1.60 ± 0.03	19.7 ± 0.2	1.05 ± 0.02	0.05 ± 0.01	43.1	0.24	0.19
RH-900	89.5 ± 0.2	1.21 ± 0.02	8.0 ± 0.1	1.21 ± 0.01	0.08 ± 0.01	51.4	0.16	0.07
RH-1000	90.0 ± 0.1	0.90 ± 0.01	8.1 ± 0.1	0.91 ± 0.01	0.09 ± 0.01	53.6	0.12	0.07
CS-raw	45.8 ± 0.3	5.98 ± 0.06	47.2 ± 0.5	0.93 ± 0.01	0.09 ± 0.01	2.6	1.57	0.77
CS-500	70.4 ± 0.3	3.39 ± 0.04	25.2 ± 0.3	0.92 ± 0.02	0.09 ± 0.01	3.1	0.57	0.27
CS-600	75.2 ± 0.2	2.79 ± 0.03	20.8 ± 0.3	1.08 ± 0.01	0.13 ± 0.01	4.0	0.45	0.21
CS-700	77.6 ± 0.2	2.06 ± 0.03	19.1 ± 0.2	1.12 ± 0.01	0.12 ± 0.01	5.0	0.32	0.18
CS-800	79.0 ± 0.2	1.26 ± 0.03	18.3 ± 0.1	1.33 ± 0.01	0.11 ± 0.01	5.7	0.19	0.17
CS-900	86.7 ± 0.1	1.01 ± 0.03	10.3 ± 0.2	1.92 ± 0.01	0.07 ± 0.01	11.8	0.14	0.09
CS-1000	86.7 ± 0.1	0.75 ± 0.02	10.4 ± 0.1	1.99 ± 0.01	0.16 ± 0.01	11.9	0.10	0.09

Fig. 5 shows the FTIR spectra of high-temperature biochars produced from RH and CS. Six distinctive absorption bands are observed in the biochars: -OH (3100–3500 cm^{-1}), -CH_3 and -CH_2- (2850–3030 cm^{-1}), C═O (1500–1750 cm^{-1}), C-O (1000–1400 cm^{-1}), and C-H (550–700 cm^{-1}). The -OH groups in the high-temperature biochars gradually decrease as the temperature increases, with the peak intensity attributed to dehydration reactions involving parallel and consecutive processes. The sustained presence of the peak associated with H_2O at high temperatures explains the continuous rise in H_2O ion intensity over 800°C. The C═O peak corresponds to carbonyl and carboxyl groups present in the conjugated aromatic carbons, indicating the existence of oxygen-containing functional groups in the high-temperature biochars.

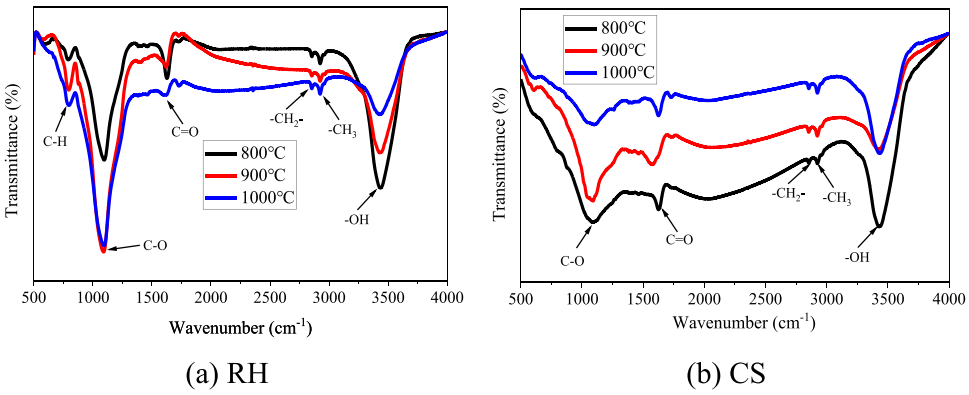

Fig. 5. FTIR spectrogram of the biochar.

It also correlates with the increasing trend of CO_2 emissions as the temperature increases. The higher ash content in RH, along with the presence of alkali and alkaline earth metal elements (AAEMs), contributes to the breakdown of interrelated cross-linked structures within the biomass [39], resulting in an increasing trend of the C═O peak in RH chars as the temperature rises. The peak observed at 1090 cm^{-1} is commonly attributed to the stretching vibration of C-O, and its high intensity suggests that it is the main source of CO generated during high-temperature pyrolysis. The rapid decline in oxygen content between 800 and 900°C can be attributed to this phenomenon. The remaining functional groups have relatively lower absorption intensities than CO, highlighting CO as the dominant gas product during high-temperature pyrolysis. The presence of the C-H peak indicates the existence of aromatic CH bonding and a significant increase in bending intensity. RH chars display minimal peak intensity, while CS chars show almost no presence, suggesting that the aromatic structures in the high-temperature pyrolysis-derived chars have achieved stability and tend towards graphitization. Moreover, the absence of peaks representing C═C stretching within the 1800–1650 cm^{-1} range provides further evidence of the degradation of aliphatic carbon side chains and bridging bonds under high temperatures. It signifies the advancement of the primary carbon framework towards graphitization. This perspective

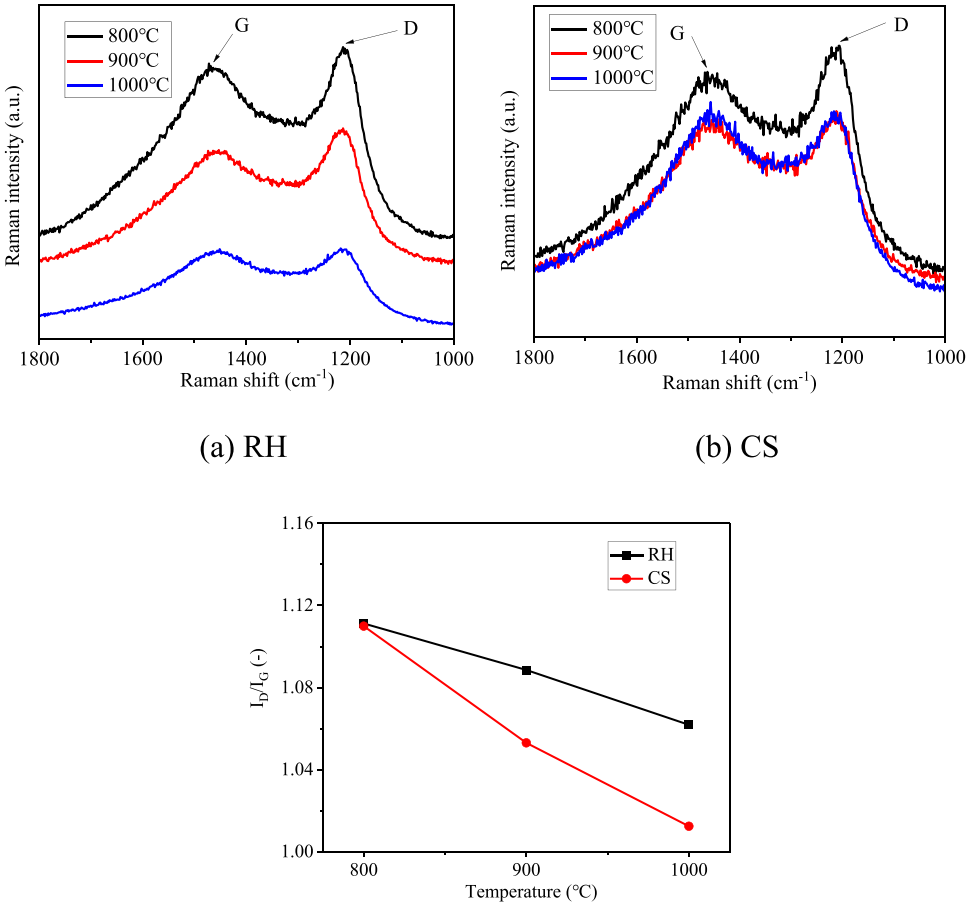

Fig. 6. Raman spectrogram of the biochar.

is further corroborated by the Raman spectra depicted in Fig. 6. The D-band (1320 cm^{-1}) signifies additional structural flaws present in highly disordered carbon materials, while the G-band (1590 cm^{-1}) signifies structurally uniform aromatic rings. The reduction in the intensity ratio of the two characteristic peaks (I_D/I_G) suggests that the lattice structure of biochar is more intact, exhibiting fewer structural defects and higher levels of graphitization.

These results are consistent with experiments conducted by various researchers. Wang et al. [40] conducted a comprehensive study on biochar in the temperature range of 800–1200°C using Raman spectroscopy, FTIR, and XPS and identified the existence of C═O and C-O functional groups. Wu et al. [41] observed an oxygen content exceeding 20% in citrus peel char at 900°C, attributing it to the significant presence of oxygen functional groups. These findings further validate that oxygen-containing substances cannot be entirely converted at 800°C, leading to their persistence in the solid biomass residues generated through high-temperature pyrolysis.

4. Modeling section

4.1. Modeling Approach

A detailed kinetic model is essential for understanding the high-temperature pyrolysis process and its practical applications. In this study, the biomass pyrolysis model CRECK-S-B proposed by Debiagi et al. [42] is adopted. The model characterizes biomass samples as varying combinations of reference components that represent the molecular structure of cellulose, hemicellulose, lignin, and extractives in real biomasses. A multi-step kinetic model describes the decomposition of each reference component using global, irreversible, and apparent first-order reactions. The model is composed of 59 reactant and product species in a total of 32 chemical reactions. Volatiles are represented by 29 realistic and lumped chemical species, encompassing permanent gases and condensable materials. Additionally, competing reactions with varying selectivities at different temperatures are considered and describe the different pyrolysis pathways. Simulation of the pyrolysis processes and sensitivity analysis is performed with the OpenSMOKE ++ Suite [43], predicting the samples' mass loss profiles, the yields of biochar, and their elemental compositions.

In this work, a large set of experimental data reported in the literature is collected and organized into a database available in the first supplemental material (SM1). The database contains the biomass composition, pyrolysis conditions, char yields, and char composition. TGA is a crucial indicator for model evaluation. The TGA data for different raw materials and heating rate conditions from the literature are compared with simulation results, attached in SM2.

4.2. CRECK-S-B kinetic model

The CRECK-S-B comprehensive model is subsequently discussed and updated based on the novel experimental results. In this model, the composition and mass fraction of each biochar residue are considered, and the accuracy of predictions is verified by calculating the C, H, and O element contents. Fig. 7 shows the comparison of C/H/O contents between the experiments and the CRECK-S-B model. Experimental data are normalized and corrected to ensure a total sum of 100% for C, H, and O. As reported [42], the relative errors for all elements are within 10%, and the CRECK-S-B model exhibits excellent predictive performance at temperatures below 800°C. However, under high-temperature conditions, the carbon content exceeds the experimental values, while oxygen and hydrogen contents significantly fall below the experimental values, with oxygen approaching 0%. Based on the test results presented in this paper and previous studies on the structure and functional groups of biochar [44–46], high-temperature biochar should contain some oxygen elements. This suggests limitations in the model to predict the conversion of oxygen-containing substances under high-temperature conditions, leading to discrepancies in the predicted results.

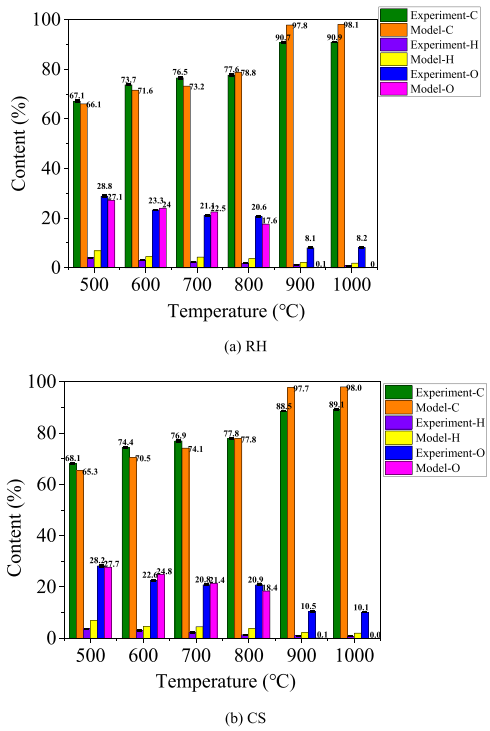

Fig. 7. Comparison of experimental data and CRECK-S-B model predictions.

To further investigate this hypothesis, Fig. 8 shows a statistical analysis comparing experimental results in the database from pyrolysis experiments above 800°C with simulated results. Out of 95 cases, 40% of the experimental results showed oxygen contents between 1% and 5%, while 35.8% fell within the 5–10% range. Only 7.37% of the experimental results indicated oxygen contents below 1%, whereas the model predicted oxygen contents below 1% in 97.9% of the cases. Therefore, the main modification discussed in this work focuses on reducing the conversion of oxygen-containing biochar functionalities at high temperatures to increase the oxygen content in biochar, achieving better agreement with experimental results. It is important to emphasize that the kinetic model of biomass pyrolysis in CRECK-S-B is continuously revised and improved to incorporate newly available experimental data [34,47].

In the CRECK-S-B model, the solid species having the name code as G $\{C_xH_yO_z\}$ represent metaplastic species and chemical functional groups attached to the nascent biochar during biomass pyrolysis. In particular, the species G$\{COH_2\}$ strongly influences the oxygen content in biochar.

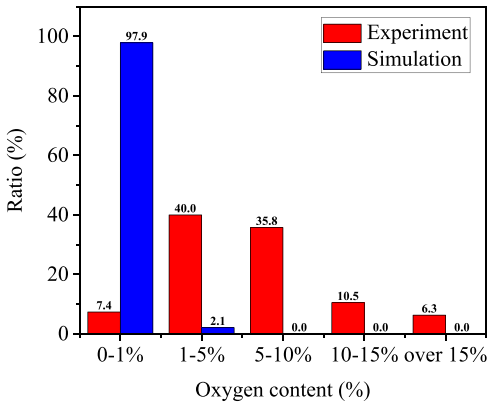

Fig. 8. Oxygen content statistics from database and model predictions.

This species decomposes following the reaction (R30):

$$G\{CH2O\} \rightarrow 0.8CO + 0.8H2 + 0.2H2O + 0.2CHAR$$

which leads to a strong decrease in oxygen content in the residual solid biochar composition at medium-high temperatures. Since the only solid product of this reaction is species CHAR (pure carbon), no residual oxygen is left in the solid after the complete decomposition of species G$\{COH_2\}$. Details on the role and decomposition of each G{} type species can be found elsewhere [42]. For these purposes, the sensitivity to the decomposition reaction of G$\{COH_2\}$ is analyzed with the brute force method. Fig. 9 shows the results of reaction rate parameters. At low temperatures, the changes in reaction rate had no significant impact on the results. However, as the pyrolysis temperature exceeds 700°C, an increased reaction rate leads to a higher production of small molecular gas products. The inflection point, where the oxygen content rapidly decreased, shifted earlier, accelerating the conversion of oxygen into biochar. By 900°C, the presence of oxygen becomes almost negligible. Nonetheless, statistical analysis indicates that the oxygen content in biochar typically falls within the range of 1–10% for pyrolysis temperatures above 800°C. Consequently, Reaction 30 is modified, including the formation of G$\{CO_{stiff}\}$, which is only released at higher temperatures as CO in the new reaction 32, and some of it remains in a new oxygen-containing biochar species (CHARO) in the new reaction 33. According to experimental results and evidence from the references [24, 40,45], G$\{CO_{stiff}\}$ is defined as solid residues containing C═O double bonds, representing carbonyl and carboxyl functional groups.

$$G\{CH2O\} \rightarrow 0.4CO + 0.8H2 + 0.2H2O + 0.2CHAR + 0.4\{CO_{stiff}\}\ k = 1.0 \times 10^{9} e^{-0.1409 \cdot T} \quad \text{(R32)}$$

$$G\{CO_{stiff}\} \rightarrow 0.8CO + 0.2CHAR_O\ k = 1.8 \times 10^{8} e^{-0.1279 \cdot T} \quad \text{(R33)}$$

The whole mechanism is shown in supplemental material 3.

The modification is implemented to enhance the activation energy required for the conversion of oxygen-containing solid products, thereby improving the accuracy of oxygen content prediction in the model while maintaining previous agreements.

4.3. Model validation

TGA is a valuable tool for analyzing the composition, thermal stability, decomposition behavior, and mass-related information of pyrolysis processes. It also serves as a good indicator for evaluating the performance of a model. The simulation results from the updated model are compared to the experimental TGA (Fig. 10). The model accurately captures the experimental trends, with the predicted mass loss closely matching the experimental data. Particularly, at pyrolysis temperatures above 800°C, the updated model slightly reduces the mass loss rate, resulting in improved agreement with the experimental findings. These changes in the conversion process of oxygen-containing solid materials suggest the presence of residual oxygen functional groups within the solid products in this temperature range. To further showcase the performance of the new model, several representative examples are selected from the database, including different biomass types and varying heating rates for the same biomass. Fig. 11 presents the comparison of TGA data, where heating rates range from 1 ℃/min to 200 ℃/min [48,49], thus illustrating the wide range reliability of the new model. Additional comparisons of TGA data for different feedstocks and heating rate conditions are available in the SM2.

Accurately predicting char yield and elemental composition is crucial as it affects the continuous reaction behavior during combustion

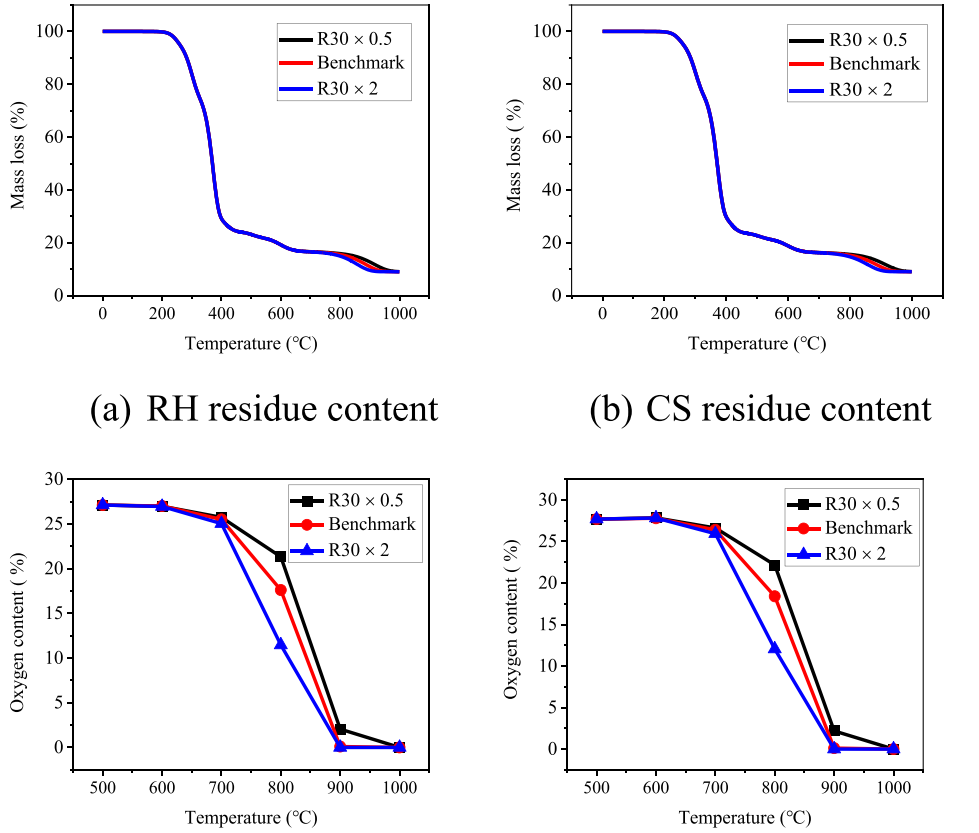

Fig. 9. Sensitivity analysis.

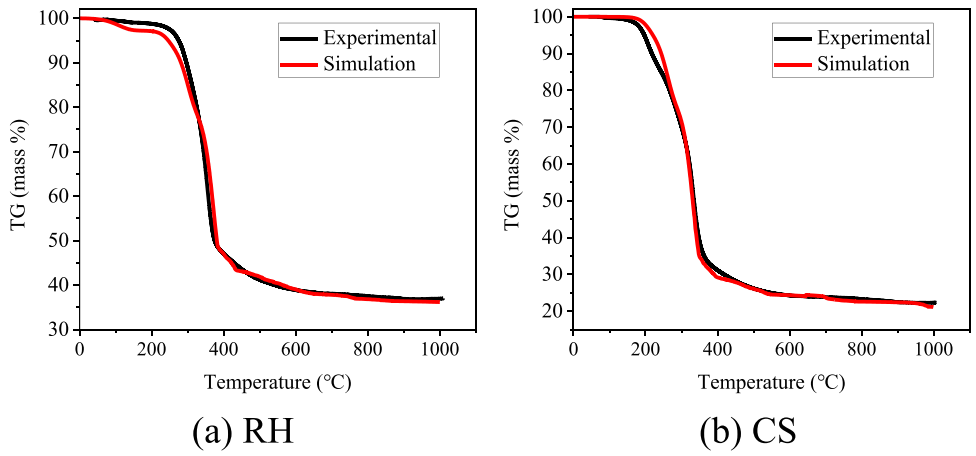

Fig. 10. Comparison of experimental TGA data and predictions of the proposed model.

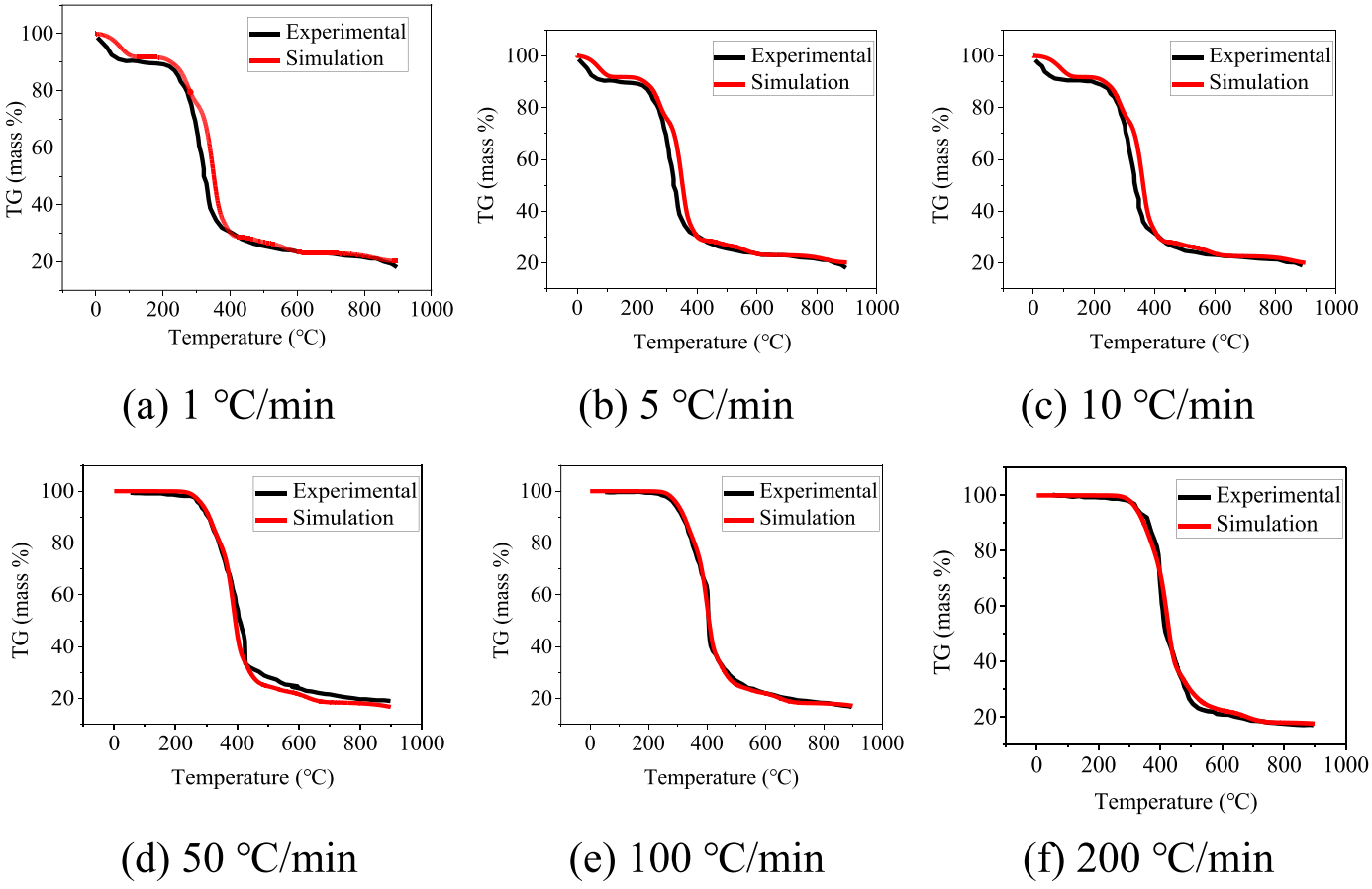

Fig. 11. Comparison of representative TGA examples and predictions of the proposed model. (a), (b), (c): Horse manure [48], (d), (e), (f): Jerusalem artichoke [49].

and gasification processes. Fig. 12 presents a comparison between experimental data and predicted values for char yield and CHO content, respectively. The results highlight the high accuracy of the new model in predicting char yield, with a relative error of less than 5%. Compared to the previous model, the updated model shows a slight increase in char yield at high temperatures, resulting in reduced relative errors for RH from 10.3% to 2.2% and for CS from 12.6% to 3.6%. Importantly, the char yield is unaffected by variations in biomass ash content. In terms of elemental composition, the modified model maintains the original accuracy at temperatures below 800°C. However, at high temperatures, the new model accurately predicts a decrease in carbon content and a reasonable increase in oxygen content.

Fig. 13 demonstrates the effectiveness of the proposed improvements, with additional comparisons between the experimental data from the database and model predictions. The database comprises different biomass types with varying ash content in the raw material, along with experimental results obtained at different pyrolysis durations. The specific experimental conditions are as follows:

(1) Pyrolysis of wood chips and rice straw in a batch-type vertical retort furnace at varying temperatures (400, 600, 800, and 1000℃) at a heating rate of 10 ℃/min for 1 hour [27]. (Fig. 13 (a) (b))

(2) Pyrolysis of pine sawdust in a fixed bed reactor at 950℃ for

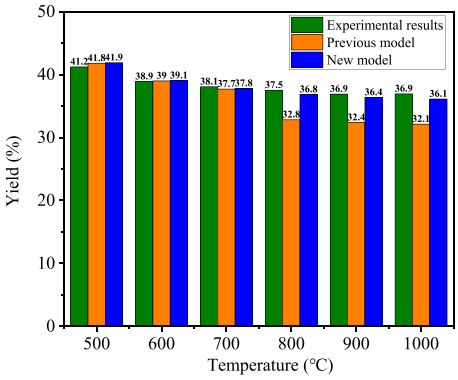

(a) RH char yield

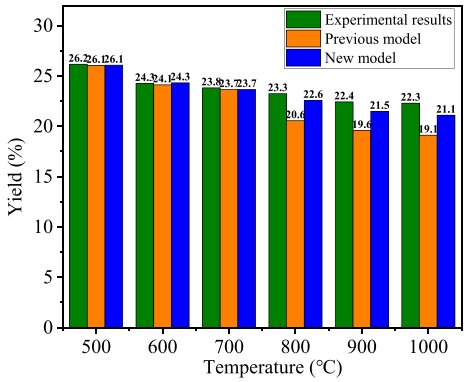

(b) CS char yield

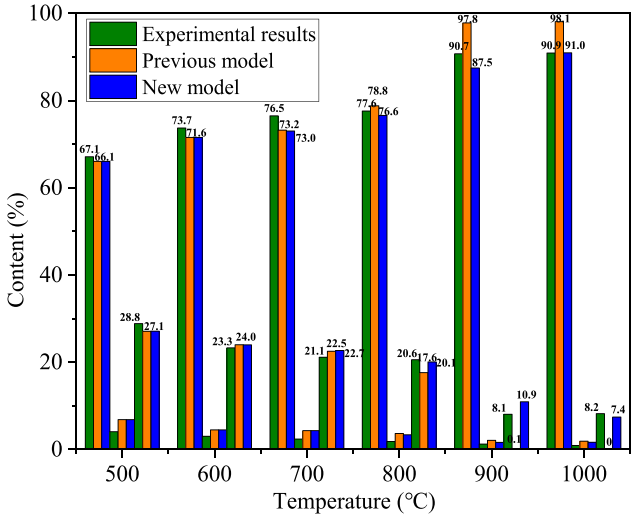

(c) RH C/H/O content

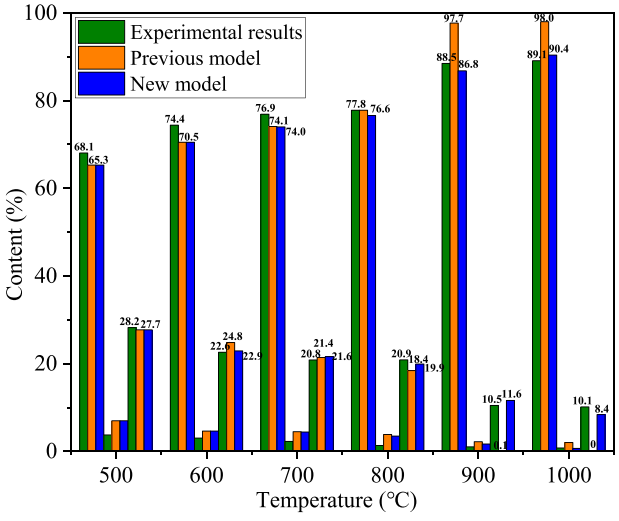

(d) CS C/H/O content

Fig. 12. Comparison of experimental data and predictions of the different model versions.

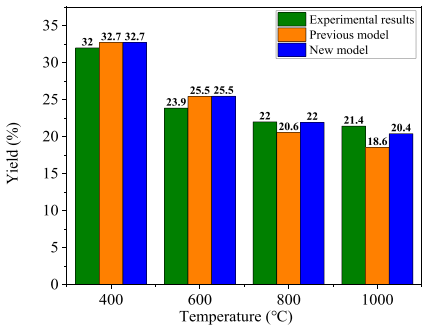

(a) Wood Chips char yield [27]

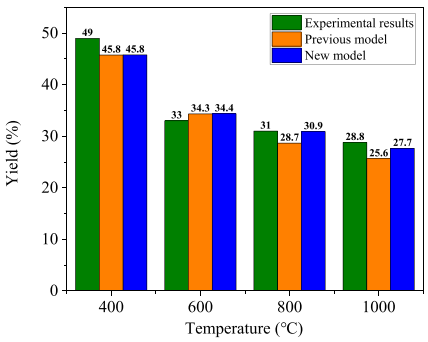

(b) Rice Straw char yield [27]

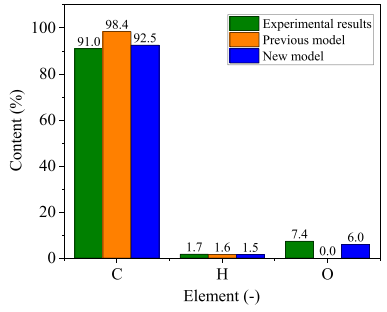

(c) Pine Sawdust C/H/O content [51]

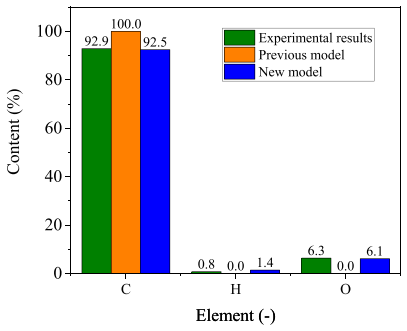

(d) Sugarcane Bagasse C/H/O content [52]

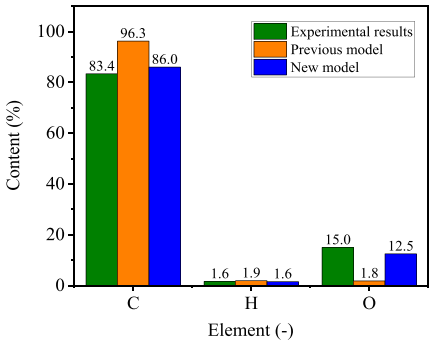

(e) Sawdust C/H/O content [53]

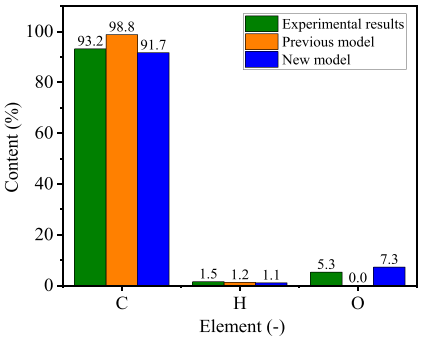

(f) Rice Husk C/H/O content [54]

Fig. 13. Comparison of representative examples in the database and predictions of the different model versions.

150 min [50]. (Fig. 13 (c))

(3) Pyrolysis of sugarcane bagasse at 40 ℃/min to 1000℃ [51]. (Fig. 12 (d))

(4) Pyrolysis of sawdust in a fixed-bed quartz tubular reactor at a heating rate of 200 ℃/min and residence time of 5 min at the final temperature of 900℃ [52]. (Fig. 13 (e))

(5) Pyrolysis of rice husk at 1000℃ for 150 min [53]. (Fig. 13 (f))

The new model exhibits higher accuracy in predicting the elemental composition and char yield of biochar residues at high temperatures. Although the char yield at high temperatures is slightly lower than the experimental results, the error is within an acceptable range. The SM1 contains a comprehensive comparison of the model predictions with 376 sets of experimental data from the database.

Fig. 14 provides the statistical comparison of all experimental data from the comprehensive database, with a criterion of relative error not exceeding 10% as the accuracy standard. It is important to acknowledge that some discrepancies in predicting experimental data may arise due to simplifications in biomass characterization and pyrolysis models. Furthermore, uncertainties exist in the experimental setup, including incomplete knowledge of biomass sources and composition, as well as insufficient descriptions of reactors and operating conditions. Nonetheless, an accuracy rate surpassing 80% sufficiently attests to the capability of the updated CRECK-S-B model to provide a simple yet adaptable computational approach for describing the intricate behavior of pyrolysis products.

5. Conclusion

In this study, the kinetics of high-temperature biomass pyrolysis are investigated using experimental and modeling approaches. The

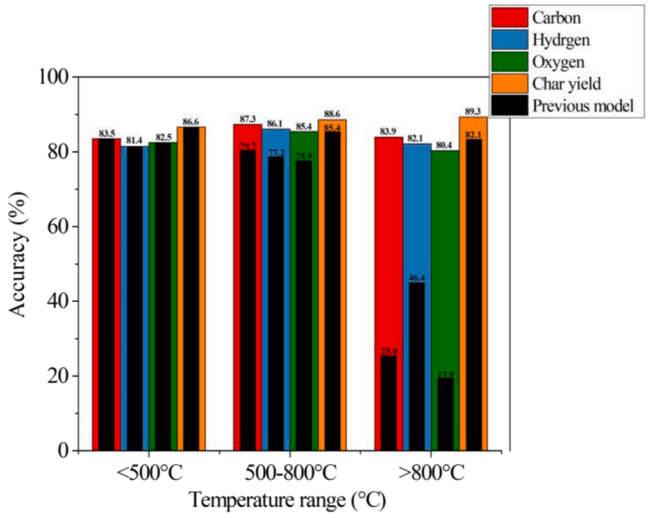

Fig. 14. C/H/O and char yield content accuracy statistics from the database.

pyrolysis processes of RH and CS are analyzed using TGA-MS, revealing distinct thermal behaviors at high temperatures. MS quantitative analysis of gaseous volatile compounds demonstrates an increased release of H_2O and CO during high-temperature pyrolysis. The two biomass samples exhibit mass losses of 1.1% and 1.5%, respectively, at temperatures exceeding 700°C, accompanied by a rapid loss of oxygen content in the solid residue. FITR results confirm that this increase is attributed to the stretching vibration of C-O bonds and the conversion of -OH groups. The remaining oxygen primarily exists as carbonyl and carboxyl groups. The CRECK-S-B biomass pyrolysis model was updated, and the revised comprehensive pyrolysis kinetics model addresses limitations in predicting oxygen content and converting oxygenated compounds at high temperatures. The accuracy of the model is validated through the comparison with experimental data and an extensive literature database. The updated model demonstrates significantly enhanced prediction accuracy for pyrolysis temperatures above 800°C. TGA curves closely matched experimental data, providing a more accurate characterization of residual biochar yield and elemental composition. The maximum relative errors in biochar yield prediction decrease significantly, from 10.3% to 2.2% and from 12.6% to 3.6%, respectively. Notably, the relative error in predicting oxygen content decreases from over 90% to within 10%. It is possible to observe an accuracy of over 80% in the prediction of pyrolysis results (including torrefaction) across the temperature range of 200–1000°C, expanding its applicability range. Additionally, a comprehensive database comprising pyrolysis experiments conducted over the past decade is established, encompassing component analysis for both biomass and biochar and experimental conditions. The results allow a better understanding of biomass high-temperature pyrolysis and provide a theoretical foundation for designing heat conversion reactors and effectively utilizing biochar.

CRediT authorship contribution statement

Tiziano Faravelli: Supervision, Resources, Project administration. **Ming Zhai:** Supervision, Funding acquisition. **Muhammad Ahsan Amjed:** Software. **Paulo Debiagi:** Writing – review & editing, Conceptualization. **Xun Zou:** Writing – original draft, Investigation, Data curation.

Declaration of Competing Interest

No conflict of interest exists in the submission of the manuscript entitled "**Impact of high-temperature biomass pyrolysis on biochar formation and composition**", and the manuscript is approved by all authors for publication.

Data Availability

Data will be made available on request.

Acknowledgment

This work was supported by the National Natural Science Foundation of China (Grant No.: 51976049) and Heilongjiang Province key research and development program (Grant No. JD22A018). Xun Zou is sponsored by China Scholarship Council (Grant NO.: 202206120144)

Activity of Muhammad Ahsan Amjed and Tiziano Faravelli is funded by the European Union (PYSOLO Project n. 101118270). Views and opinions expressed are however those of the author(s) only and do not necessarily reflect those of the European Union or the European Health and Digital Executive Agency (HADEA). Neither the European Union nor the granting authority can be held responsible for them.

P. Debiagi and T. Faravelli acknowledge the financial support from DFG – CRC 129 "Oxyflame" (project number 215035359).

Appendix A. Supporting information

Supplementary data associated with this article can be found in the online version at doi:10.1016/j.jaap.2024.106463.

References

[1] H. Sun, Z. Luo, W. Wang, et al., Porosity roles of micro-mesostructured ZSM-5 in catalytic fast pyrolysis of cellulolytic enzyme lignin for aromatics, Energy Convers. Manag. 247 (2021) 114753, https://doi.org/10.1016/j.enconman.2021.114753.
[2] X. Zou, M. Zhai, D. Yang, et al., New insights into the mechanism of biomass char steam gasification process by oxygen-containing functional group as aromatic carbon boundaries: Experimental and DFT study, Chem. Eng. J. 465 (2023) 142947, https://doi.org/10.1016/j.cej.2023.142947.
[3] Y. Ma, Z. Ge, F. Li, et al., Pyrolysis and CO2 gasification of biomass in high-temperature stage microscope: morphological evolution and thermal behaviors, Combust. Flame 245 (2022) 112387, https://doi.org/10.1016/j.combustflame.2022.112387.
[4] Z. Zha, Z. Ge, S. Wang, et al., Biomass combustion behaviors based on online monitoring system: morphological, thermodynamic and kinetic analysis, Combust. Flame 252 (2023) 112750, https://doi.org/10.1016/j.combustflame.2023.112750.
[5] J. Lee, S. Kim, S. You, et al., Bioenergy generation from thermochemical conversion of lignocellulosic biomass-based integrated renewable energy systems, Renew. Sustain. Energy Rev. 178 (2023) 113240, https://doi.org/10.1016/j.rser.2023.113240.
[6] I.M.T. Usman, Y.C. Ho, L. Baloo, et al., A comprehensive review on the advances of bioproducts from biomass towards meeting net zero carbon emissions (NZCE), Bioresour. Technol. (2022) 128167, https://doi.org/10.1016/j.biortech.2022.128167.
[7] K. Tokimatsu, R. Yasuoka, M. Nishio, Global zero emissions scenarios: The role of biomass energy with carbon capture and storage by forested land use, Appl. Energy 185 (2017) 1899–1906, https://doi.org/10.1016/j.apenergy.2015.11.077.
[8] S. Wang, K. Wu, J. Yu, et al., Kinetic and thermodynamic analysis of biomass catalytic pyrolysis with nascent biochar in a two-stage reactor, Combust. Flame 251 (2023) 112671, https://doi.org/10.1016/j.combustflame.2023.112671.
[9] Sri Shalini S, Palanivelu K, Ramachandran A, et al., Biochar from biomass waste as a renewable carbon material for climate change mitigation in reducing greenhouse gas emissions—A review, Biomass Convers. Biorefinery 11 (2021) 2247–2267, https://doi.org/10.1007/s13399-020-00604-5.
[10] E. Ranzi, P.E.A. Debiagi, A. Frassoldati, Mathematical modeling of fast biomass pyrolysis and bio-oil formation. Note I: kinetic mechanism of biomass pyrolysis, ACS Sustain. Chem. Eng. 5 (4) (2017) 2867–2881, https://doi.org/10.1021/acssuschemeng.6b03096.
[11] K.N. Yogalakshmi, P. Sivashanmugam, S. Kavitha, et al., Lignocellulosic biomass-based pyrolysis: a comprehensive review, Chemosphere 286 (2022) 131824, https://doi.org/10.1016/j.chemosphere.2021.131824.
[12] S. Wang, X. Guo, K. Wang, et al., Influence of the interaction of components on the pyrolysis behavior of biomass, J. Anal. Appl. Pyrolysis 91 (1) (2011) 183–189, https://doi.org/10.1016/j.jaap.2011.02.006.
[13] S.K. Bhatia, A.K. Palai, A. Kumar, et al., Trends in renewable energy production employing biomass-based biochar, Bioresour. Technol. 340 (2021) 125644, https://doi.org/10.1016/j.biortech.2021.125644.
[14] Y. Huang, S. Xia, J. Lyu, et al., Highly efficient removal of aqueous Hg2+ and CH3Hg+ by selective modification of biochar with 3-mercaptopropyltrimethoxysilane, Chem. Eng. J. 360 (2019) 1646–1655, https://doi.org/10.1016/j.cej.2018.10.231.

[15] S.B. Patwardhan, S. Pandit, P.K. Gupta, et al., Recent advances in the application of biochar in microbial electrochemical cells, Fuel 311 (2022) 122501, https://doi.org/10.1016/j.fuel.2021.122501.
[16] J. Lang, L. Matějová, A.K. Cuentas-Gallegos, et al., Evaluation and selection of biochars and hydrochars derived from agricultural wastes for the use as adsorbent and energy storage materials, J. Environ. Chem. Eng. 9 (5) (2021) 105979, https://doi.org/10.1016/j.jece.2021.105979.
[17] W.J. Liu, H. Jiang, H.Q. Yu, Emerging applications of biochar-based materials for energy storage and conversion, Energy Environ. Sci. 12 (6) (2019) 1751–1779, https://doi.org/10.1039/C9EE00206E.
[18] E. Kantarelis, P. Donaj, W. Yang, et al., Sustainable valorization of plastic wastes for energy with environmental safety via High-Temperature Pyrolysis (HTP) and high-temperature steam gasification (HTSG), J. Hazard. Mater. 167 (1-3) (2009) 675–684, https://doi.org/10.1016/j.jhazmat.2009.01.036.
[19] A. Çağlar, A. Demirbaş, Hydrogen rich gas mixture from olive husk via pyrolysis, Energy Convers. Manag. 43 (1) (2002) 109–117, https://doi.org/10.1016/S0196-8904(01)00012-7.
[20] C.E. Efika, J.A. Onwudili, P.T. Williams, Influence of heating rates on the products of high-temperature pyrolysis of waste wood pellets and biomass model compounds, Waste Manag. 76 (2018) 497–506, https://doi.org/10.1016/j.wasman.2018.03.021.
[21] X. Zou, L. Guo, H. Li, et al., Density functional theory study on N element migration during the secondary cracking of rice husk tar, J. Energy Inst. 102 (2022) 337–349, https://doi.org/10.1016/j.joei.2022.04.005.
[22] S. Septien, S. Valin, C. Dupont, et al., Effect of particle size and temperature on woody biomass fast pyrolysis at high temperature (1000–1400C), Fuel 97 (2012) 202–210, https://doi.org/10.1016/j.fuel.2012.01.049.
[23] A. Paethanom, K. Yoshikawa, Influence of pyrolysis temperature on rice husk char characteristics and its tar adsorption capability, Energies 5 (12) (2012) 4941–4951, https://doi.org/10.3390/en5124941.
[24] X. Zou, M. Zhai, B. Wang, et al., Molecular-scale elucidating of lignocellulose biomass char steam gasification for ultimately converting to syngas, Fuel Process. Technol. 236 (2022) 107430, https://doi.org/10.1016/j.fuproc.2022.107430.
[25] J. Zhang, J. Liu, R. Liu, Effects of pyrolysis temperature and heating time on biochar obtained from the pyrolysis of straw and lignosulfonate, Bioresour. Technol. 176 (2015) 288–291, https://doi.org/10.1016/j.biortech.2014.11.011.
[26] P. Pariyar, K. Kumari, M.K. Jain, et al., Evaluation of change in biochar properties derived from different feedstock and pyrolysis temperature for environmental and agricultural application, Sci. Total Environ. 713 (2020) 136433, https://doi.org/10.1016/j.scitotenv.2019.136433.
[27] A. Anand, S. Gautam, L.C. Ram, Feedstock and pyrolysis conditions affect suitability of biochar for various sustainable energy and environmental applications, J. Anal. Appl. Pyrolysis 170 (2023) 105881, https://doi.org/10.1016/j.jaap.2023.105881.
[28] G.R. Surup, H.K. Nielsen, M. Heidelmann, et al., Characterization and reactivity of charcoal from high temperature pyrolysis (800–1600C), Fuel 235 (2019) 1544–1554, https://doi.org/10.1016/j.fuel.2018.08.092.
[29] S. Wang, G. Dai, H. Yang, et al., Lignocellulosic biomass pyrolysis mechanism: s state-of-the-art review, Prog. Energy Combust. Sci. 62 (2017) 33–86, https://doi.org/10.1016/j.pecs.2017.05.004.
[30] J.F. Peters, S.W. Banks, A.V. Bridgwater, et al., A kinetic reaction model for biomass pyrolysis processes in Aspen Plus, Appl. Energy 188 (2017) 595–603, https://doi.org/10.1016/j.apenergy.2016.12.030.
[31] E. Ranzi, A. Cuoci, T. Faravelli, et al., Chemical kinetics of biomass pyrolysis, Energy Fuels 22 (6) (2008) 4292–4300, https://doi.org/10.1021/ef800551t.
[32] P.E.A. Debiagi, C. Pecchi, G. Gentile, et al., Extractives extend the applicability of multistep kinetic scheme of biomass pyrolysis, Energy Fuels 29 (10) (2015) 6544–6555, https://doi.org/10.1021/acs.energyfuels.5b01753.
[33] T. Faravelli, A. Frassoldati, G. Migliavacca, et al., Detailed kinetic modeling of the thermal degradation of lignins[J], Biomass Bioenergy 34 (3) (2010) 290–301, https://doi.org/10.1016/j.biombioe.2009.10.018.
[34] P.E.A. Debiagi, G. Gentile, M. Pelucchi, et al., Detailed kinetic mechanism of gas-phase reactions of volatiles released from biomass pyrolysis, Biomass Bioenergy 93 (2016) 60–71, https://doi.org/10.1016/j.biombioe.2016.06.015.
[35] Y.N. Xiao, F. Niu, S.F. Fu, The Reductive method of copper and the optimization of oxygen dosing in the reduction tube of Vario EL III elemental analyzer, Adv. Mater. Res. 915 (2014) 1070–1073, https://doi.org/10.4028/www.scientific.net/AMR.915-916.1070.
[36] F.X. Collard, J. Blin, A review on pyrolysis of biomass constituents: Mechanisms and composition of the products obtained from the conversion of cellulose, hemicelluloses and lignin, Renew. Sustain. Energy Rev. 38 (2014) 594–608, https://doi.org/10.1016/j.rser.2014.06.013.
[37] G. Özsin, A.E. Pütün, Kinetics and evolved gas analysis for pyrolysis of food processing wastes using TGA/MS/FT-IR, Waste Manag. 64 (2017) 315–326, https://doi.org/10.1016/j.wasman.2017.03.020.
[38] K. Crombie, O. Mašek, S.P. Sohi, et al., The effect of pyrolysis conditions on biochar stability as determined by three methods, Gcb Bioenergy 5 (2) (2013) 122–131, https://doi.org/10.1111/gcbb.12030.
[39] D. Feng, Y. Zhao, Y. Zhang, et al., Catalytic mechanism of ion-exchanging alkali and alkaline earth metallic species on biochar reactivity during CO2/H2O gasification, Fuel 212 (2018) 523–532, https://doi.org/10.1016/j.fuel.2017.10.045.
[40] X. Wang, M. Zhai, H. Guo, et al., High-temperature pyrolysis of biomass pellets: the effect of ash melting on the structure of the char residue, Fuel 285 (2021) 119084, https://doi.org/10.1016/j.fuel.2020.119084.
[41] Y. Wu, Y. Pang, Y. Chen, et al., Study on the steam gasification reaction of biomass char under the synergistic effect of Ca-Fe: Analysis of kinetic characteristics, Int. J. Energy Res. 45 (5) (2021) 7814–7828, https://doi.org/10.1002/er.6366.
[42] P. Debiagi, G. Gentile, A. Cuoci, et al., A predictive model of biochar formation and characterization, J. Anal. Appl. Pyrolysis 134 (2018) 326–335, https://doi.org/10.1016/j.jaap.2018.06.022.
[43] A. Cuoci, A. Frassoldati, T. Faravelli, et al., OpenSMOKE++: An object-oriented framework for the numerical modeling of reactive systems with detailed kinetic mechanisms, Comput. Phys. Commun. 192 (2015) 237–264, https://doi.org/10.1016/j.cpc.2015.02.014.
[44] C. Peng, Y. Zhai, Y. Zhu, et al., Investigation of the structure and reaction pathway of char obtained from sewage sludge with biomass wastes, using hydrothermal treatment, J. Clean. Prod. 166 (2017) 114–123, https://doi.org/10.1016/j.jclepro.2017.07.108.
[45] C. Guizani, K. Haddad, L. Limousy, et al., New insights on the structural evolution of biomass char upon pyrolysis as revealed by the Raman spectroscopy and elemental analysis, Carbon 119 (2017) 519–521, https://doi.org/10.1016/j.carbon.2017.04.078.
[46] M.J. Wornat, R.H. Hurt, N.Y.C. Yang, et al., Structural and compositional transformations of biomass chars during combustion, Combust. Flame 100 (1-2) (1995) 131–143, https://doi.org/10.1016/0010-2180(94)00055-W.
[47] E. Ranzi, M. Corbetta, F. Manenti, et al., Kinetic modeling of the thermal degradation and combustion of biomass, Chem. Eng. Sci. 110 (2014) 2–12, https://doi.org/10.1016/j.ces.2013.08.014.
[48] B. Wang, F. Xu, P. Zong, et al., Effects of heating rate on fast pyrolysis behavior and product distribution of Jerusalem artichoke stalk by using TG-FTIR and Py-GC/MS, Renew. Energy 132 (2019) 486–496, https://doi.org/10.1016/j.renene.2018.08.021.
[49] C.T. Chong, G.R. Mong, J.H. Ng, et al., Pyrolysis characteristics and kinetic studies of horse manure using thermogravimetric analysis, Energy Convers. Manag. 180 (2019) 1260–1267, https://doi.org/10.1016/j.enconman.2018.11.071.
[50] J. He, Z. Yang, M. Guo, et al., Experimental study on the key factors affecting the gasification performance between different biomass: Compare citrus peel with pine sawdust, Int. J. Hydrog. Energy 47 (71) (2022) 30428–30439, https://doi.org/10.1016/j.ijhydene.2022.07.004.
[51] K. Jayaraman, I. Gokalp, S. Petrus, et al., Energy recovery analysis from sugar cane bagasse pyrolysis and gasification using thermogravimetry, mass spectrometry and kinetic models, J. Anal. Appl. Pyrolysis 132 (2018) 225–236, https://doi.org/10.1016/j.jaap.2018.02.003.
[52] T.R. Pacioni, D. Soares, M. Di Domenico, et al., Bio-syngas production from agro-industrial biomass residues by steam gasification, Waste Manag. 58 (2016) 221–229, https://doi.org/10.1016/j.wasman.2016.08.021.
[53] Y. Shu, H. Wang, J. Zhu, et al., An experimental study of heterogeneous NO reduction by biomass reburning, Fuel Process. Technol. 132 (2015) 111–117, https://doi.org/10.1016/j.fuproc.2014.12.039.